



Full paper

A waterproof, breathable nitrocellulose-based triboelectric nanogenerator for human-machine interaction

Tong Zheng^{a,1}, Guizhong Li^{a,d,*,1}, Linnan Zhang^a, Weifang Sun^a, Xiaoming Pan^a,
Taihong Chen^a, Yuanhao Wang^{c,**}, Yuqing Zhou^{a,f}, Jili Tian^{g,**}, Ya Yang^{b,e,***}

^a College of Mechanical and Electrical Engineering, Wenzhou University, Wenzhou 325035, China

^b CAS Center for Excellence in Nanoscience, Beijing Key Laboratory of Micro-nano Energy and Sensor, Beijing Institute of Nanoenergy and Nanosystems, Chinese Academy of Sciences, Beijing 101400, China

^c Hoffmann Institute of Advanced Materials, Shenzhen Polytechnic, 7098 Liuxian Boulevard, Nanshan District, Shenzhen 518055, China

^d Wenzhou University Pingyang Institute of Intelligent Manufacturing, Wenzhou 325400, China

^e School of Nanoscience and Technology, University of Chinese Academy of Sciences, Beijing 100049, China

^f College of Mechanical and Electrical Engineering, Jiaxing Nanhu University, Jiaxing 314001, China

^g School of Energy and Mechanical Engineering, Dezhou University, Dezhou 253023, China

ARTICLE INFO

Keywords:

Triboelectric nanogenerator

Nitrocellulose

Waterproofness

Breathability

Human-machine interaction

ABSTRACT

Triboelectric nanogenerators (TENGs) have attracted significant attention as a promising method for energy harvesting and self-powered sensing. In this study, we developed a waterproof, breathable nitrocellulose-based TENG for human-machine interaction. The optimal performance of modified nitrocellulose (NC) membrane was enhanced in waterproofness (water contact angle of 86.9°), breathability (water vapor transmission rate of 562.62 g/m²/d) and transparency (92%). To improve the output performance, silver nanowires (Ag NWs) were doped into the tribo-positive layer (NC) based on dielectric enhancement effect. The NC-based TENG doped with Ag NWs (NC-Ag NWs) demonstrated a 360% improvement in triboelectric performance compared to the unoptimized one. The instantaneous power density of NC-TENG can reach 0.38 W/m². Furthermore, to comprehend the mechanism underlying this enhancement, an internal capacitance model of the NC-Ag NWs was developed. Combining the triboelectric performance and physical characteristics of NC-Ag NWs, we designed a self-powered single-electrode TENG (SNC-TENG) and a double-electrode TENG matrix keyboard to facilitate real-time communication with electronic devices. This work demonstrates a feasible and simple method to fabricate high-performance TENGs and shows its potential application in the fields of wearable devices and self-powered systems.

1. Introduction

A number of smart devices and small wearable devices (SWDs) are springing up due to the rapid development of the internet of things (IoT) and artificial intelligence (AI), correspondingly, flexible electronics and sensing devices have become humans' urgent needs [1–5]. Those wearable devices can be applied in various fields, for instance, human physiological characteristics monitoring [6], tactile perception [7] and human-machine interaction (HMI) [8]. Most wearable devices are

driven by external energy sources, like batteries, however there exist problems of periodic recharge and maintenance, limited lifetime and environmental pollutions. Therefore, an urgent demand has been put forward on humans to develop a method for harvesting energy from the environment and powering wearable devices. Triboelectric nanogenerator (TENG), with simple structure and high energy conversion efficiency in low frequency, is regarded as an emerging energy conversion technique for harvesting low-frequency and irregular energy scattered around the world. Furthermore, TENG wearable devices can be

* Corresponding author at: College of Mechanical and Electrical Engineering, Wenzhou University, Wenzhou 325035, China.

** Corresponding authors.

*** Corresponding author at: CAS Center for Excellence in Nanoscience, Beijing Key Laboratory of Micro-nano Energy and Sensor, Beijing Institute of Nanoenergy and Nanosystems, Chinese Academy of Sciences, Beijing 101400, China.

E-mail addresses: liguizhong@wzu.edu.cn (G. Li), wangyuanhao@szpt.edu.cn (Y. Wang), tianjili1987@163.com (J. Tian), yayang@binn.cas.cn (Y. Yang).

¹ Contributed equally to this work

made with various triboelectric materials, such as kapton film [9], protein [10], silicone rubber [11] and cellulose [12]. Benefiting from the extensive materials selection and outstanding performance of TENG, a host of self-powered sensing and HMI devices have been created [13–18].

Nitrocellulose (NC) is a material with positive triboelectric performance, which is mainly prepared by the nitration of cellulose [19]. Besides, NC is widely used as portable diagnostic biosensors, wearable biosensors and cell-based biosensors [20–22]. Simultaneously, NC-based materials also were used to fabricate self-powered sensing devices recently [23,24]. A nitrocellulose-based self-powered alarm system was designed to detect the third-level details of latent fingerprints [23]. Besides, a human-machine interface was developed to interactive with electric devices by using nitrocellulose membrane and crepe cellulose paper [24]. Although some related works have been reported, the wearing comfort of self-powered sensing devices is still limited by its physical characteristics, such as breathability, waterproofness and transparency. Besides, the triboelectric performance of nitrocellulose-based triboelectric nanogenerator (NC-TENG) is needed to promote further.

Recently, researchers have devoted to innovate high-performance TENG with excellent wearing comfort for energy harvesting and self-powered sensing [25–29]. Several studies of breathable, waterproof and flexible TENG devices have been reported [30–33]. But there still are some limitations, such as high energy consumption in preparation [33,34] and low output performance [30,32,35]. Therefore, utilized a simple and cost-effective method for preparation of waterproof, breathable and transparent TENG with high output performance remains a great challenge. At present, dielectric enhancement effect was regarded as a promising strategy to improve the triboelectric performance by modifying the triboelectric layer with proper method [36]. There are TENGs that have been fabricated by adding nano particles in triboelectric layer therefore the performance of TENGs were enhanced greatly [37–39]. Accordingly, a method for the fabrication of TENG simultaneously considering the waterproofness, breathability, transparency, low cost, easy to preparation and high dielectric property is highly desired to enhance the performance of NC-TENG and promote its application.

In this work, we proposed a feasible strategy to fabricate a waterproof, breathable, transparent and high-performance NC-TENG through a simple and cost-effective approach. The waterproofness, breathability and transparency of pure NC have an obvious enhancement. In addition, we optimized the triboelectric performance of modified pure NC by doping Ag NWs. The open-circuit voltage and transferred charges of NC-TENG can reach 180 V, 68 nC, respectively. The internal capacitance model of NC-Ag NWs was established and the mechanism of output enhancement was analyzed. In addition, a single electrode mode NC-TENG was designed for human machine interaction. Features of human touch (such as pressures and frequencies) could be recorded at the same time. Furthermore, a double electrode matrix keyboard was designed to record and visualize the finger touch. Combined with the excellent performance of NC-Ag NWs, the NC-TENG can be used in energy harvesting, self-powered sensing and HMI.

2. Experiment section

2.1. Materials

All reagents are used as obtained without any further purification. Ethyl acetate (EA, AR) and isopropyl alcohol (IPA, AR) were purchased from MACKLIN company. Dioctyl phthalate (DOP, AR) was purchased from Wuxi Yatai United Chemical Co. Ltd. PDMS (SYLGARD™ 184) was purchased from The Dow Chemical Company (US). The dispersion liquid of Ag NWs (Length: 20 μm) 20 μm) was purchased from Jiangsu Xianfeng Nanomaterial Technology Co. Ltd. NC film (Nitrogen content: 6%; pore size: 5 μm , 2 μm , 0.8 μm and 0.15 μm) was purchased from

Shanghai Xingya Purification Materials Co. Ltd.

2.2. Fabrication of the NC-Ag NWs

As shown in Fig. 1a, firstly, a certain amount of NCs were added into the beaker with the mixed solvent that consisted of EA, IPA and DOP, the mixture was then stirred at 50 °C for 1 h. Secondly, the silver nanowire solution of isopropanol (containing Ag NWs: 5 mg/ml) was added into the mixture at the stirring state, the Ag NWs amounts of 0.25 mg, 0.75 mg, 1.25 mg, 1.75 mg and 2.25 mg, respectively. Next, the mixture of NC-Ag NWs was stirred continuously for 2 h to obtain a homogeneous mixture. Thirdly, the mixture was dropped into a glass petri dish that has been preheated with a heating table at 50 °C. Fourthly, when the solvent of the mixture was evaporated and the solute was cured, the membrane of NC-Ag NWs was peeled off from the glass petri dish and cut into proper size.

2.3. Fabrication of the PDMS

The PDMS elastomer (Dow Corning) and curing agent (Dow Corning) were added into a beaker with the ratio (w/w) of 10:1, and then the mixture was stirred with an electromagnetic stirrer for 1 h to make sure that the mixture was well-mixed. Next, the mixture was vacuumed to remove bubbles, and then the mixture was dropped on the mold within thermal curing at 80 °C for 3 h.

2.4. Fabrication of the TENGs

The fabrication process of double electrode TENG was displayed in Fig. 1b. The aluminum (Al) and conductive fabric were chosen as the electrode of PDMS and NC-Ag NWs, respectively. The top layer of TENG was composed of Al (electrode) and PDMS (negative friction layer), and the bottom layer of NC-Ag NWs (positive friction layer) was attached to the conductive fabric (electrode). Among the top and bottom layers, two PDMS cuboids acted as the supporting layer that prevented contact between PDMS and NC-Ag NWs all the time.

The SNC-TENG was composed of a piece of NC-Ag NWs (2 cm \times 2 cm) and a conductive fabric (2 cm \times 2 cm), the NC-Ag NWs (tribo-positive layer) was attached on the conductive fabric (breathable electrode). A thin PDMS (0.5 cm \times 0.5 cm) was used as tribo-negative layer and attached to finger in order to strengthen the self-powered sensing performance.

For the double electrode matrix keyboard, which could be constructed by nine connected units of small NC-TENG. As far as the whole matrix keyboard, the bottom was constituted of three Al electrodes (1.5 cm \times 8 cm). And nine pieces of PDMS (1.5 cm \times 2 cm) were divided into three parts, every three PDMS were attached to the same aluminum electrode with the same interval. Correspondingly, nine NC-Ag NWs (1.5 cm \times 1.5 cm) adhered with conductive textiles were designed as the top layer. The soft Ethylene Vinyl Acetate (EVA, 8 cm \times 8 cm) copolymer was used as the substrate. The two PDMS cuboids (1.5 cm \times 0.5 cm \times 0.5 cm) were stuck around the NC-Ag NWs, serving as supporting layer and avoiding NC-Ag NWs contacts with PDMS in bottom layer all the time.

2.5. Characterization and measurements

All the microstructures and elemental components of NC-Ag NWs in this report were characterized by scanning electron microscopy (SEM, Nova 200 NanoLab) and transmission electron microscope (TEM, G20 FEI) equipped with EDS. The surface chemical analyses of NC-Ag NWs in this report was performed by X-ray photoelectron spectrometer (XPS, PHI 5000 VersaProbe III). The crystalline structure of NC-Ag NWs was performed by X-Ray Diffraction (BRUKER, D8 Advance). The transmittance of NC-Ag NWs was measured at the range of 300–800 nm spectral region by ultraviolet-visible spectroscopy (Shimadzu, UV2600).

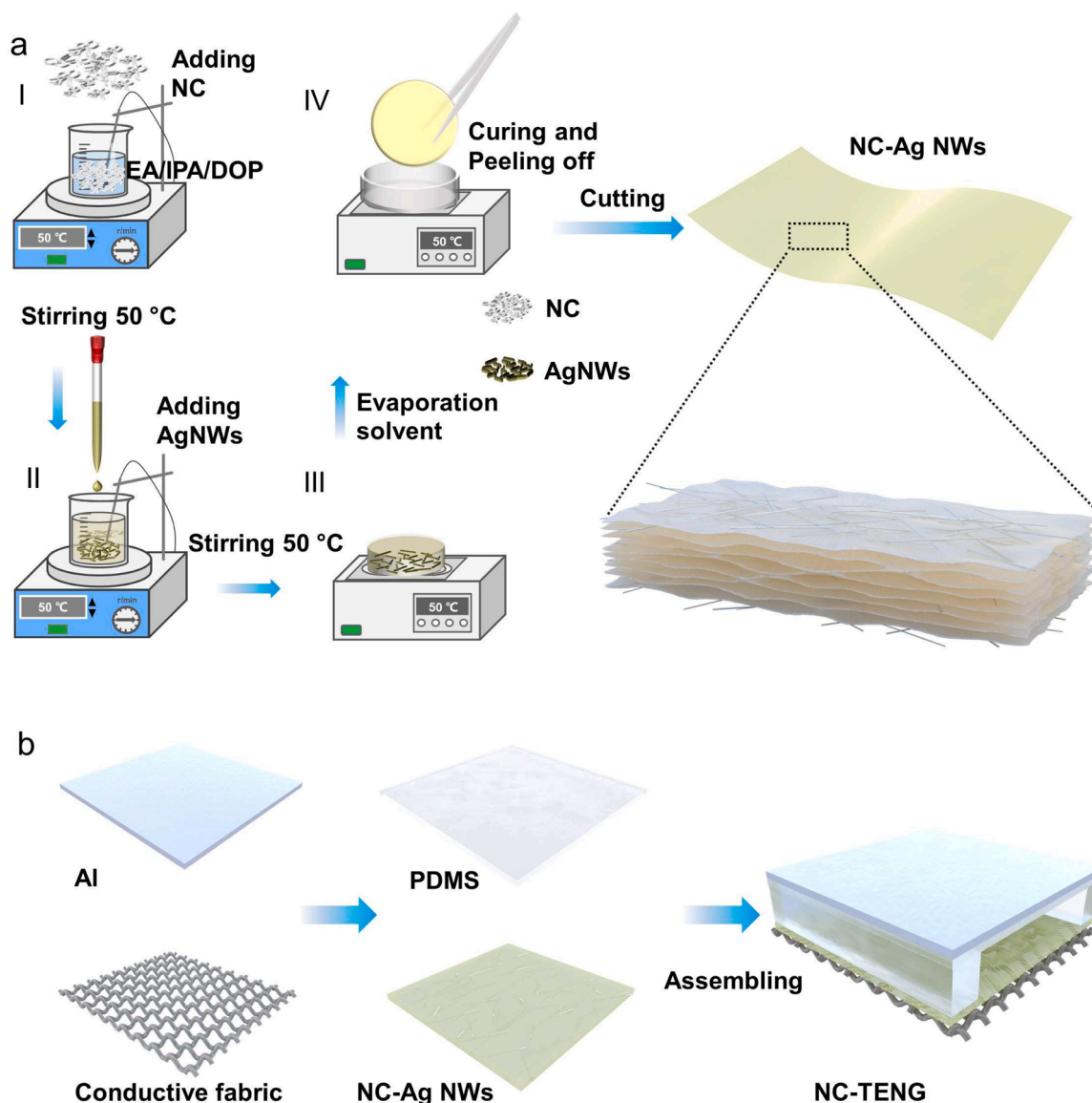


Fig. 1. Schematic diagram for NC-Ag NWs based TENG. (a) The preparation process of NC-Ag NWs. (b) The fabrication process of NC-TENG.

The Thermogravimetric analysis (TGA) was conducted with the heating from 40–600 °C and the heating rate of 10 °C/ min under nitrogen flow (PerkinElmer, Pyris Diamond TG-DTA). And the water contact angle of NC-Ag NWs was measured (LSA100, China). The relative humidity of the environment was gotten by a hygrometer (Deli, DL8840). The capacitances of NC-Ag NWs were measured using an electrochemical workstation (CHI660E). A Keithley 6514 electrometer was used to measure the open-circuit voltage, short-circuit current and the transferred charges of TENGs, and data was recorded by data acquisition card (NI, USB-6009).

3. Results and Discussion

Firstly, we investigated the waterproofness and breathability of modified NC with different pore sizes of NC film (Temperature: 293 K, relative humidity: 50%), the results indicated that the waterproofness of modified NC was improved with the decrease of the pore size of NC film (Fig. S1). But the breathability of modified NC shows a contrary trend (Fig. S2). Considering the wearing comfort of human, the NC film with the pore size of 5 μm was chosen for the investigation further. It was noted that the modified method plays a large significant part in

enhancing physical characteristics of pure NC membrane. In addition, the Ag NWs play a crucial part in improving the triboelectric performance of NC-Ag NWs, which changed the internal capacitance of the material. The NC-Ag NWs was prepared via a simple “one-pot” method. Fig. 2a displays the modified NC membrane doped with 1.25 mg Ag NWs. The surface and side scanning electron microscope (SEM) images of NC-Ag NWs are shown in Fig. 2b and Fig. 2c, respectively. Some nano/micro-pores were generated when dissolved NC membranes came into being (shown in Fig. 2b), which endowed the NC-Ag NWs with outstanding breathability. Thus, water molecules and air could pass through the membranes from bottom to top easily. Fig. 2c shown the layered structure of NC-Ag NWs, Ag NWs were distributed homogeneously and randomly in every layer. Fig. 2d exhibits the results of energy dispersive spectroscopy (EDS) of NC-Ag NWs, confirmed the Ag element in NC-Ag NWs.

To investigate the interaction mechanism between Ag NWs and NC, the morphological analysis of Ag NW was conducted with transmission electron microscope equipped (TEM) with EDS. The Ag NW can be capture clearly (Fig. 2e), and the EDS results are shown in Fig. 2f. Note that the area of Ag NW exists C, O and N element, which indicates the NC and Ag NW are inseparable in internal structure of NC-Ag NWs.

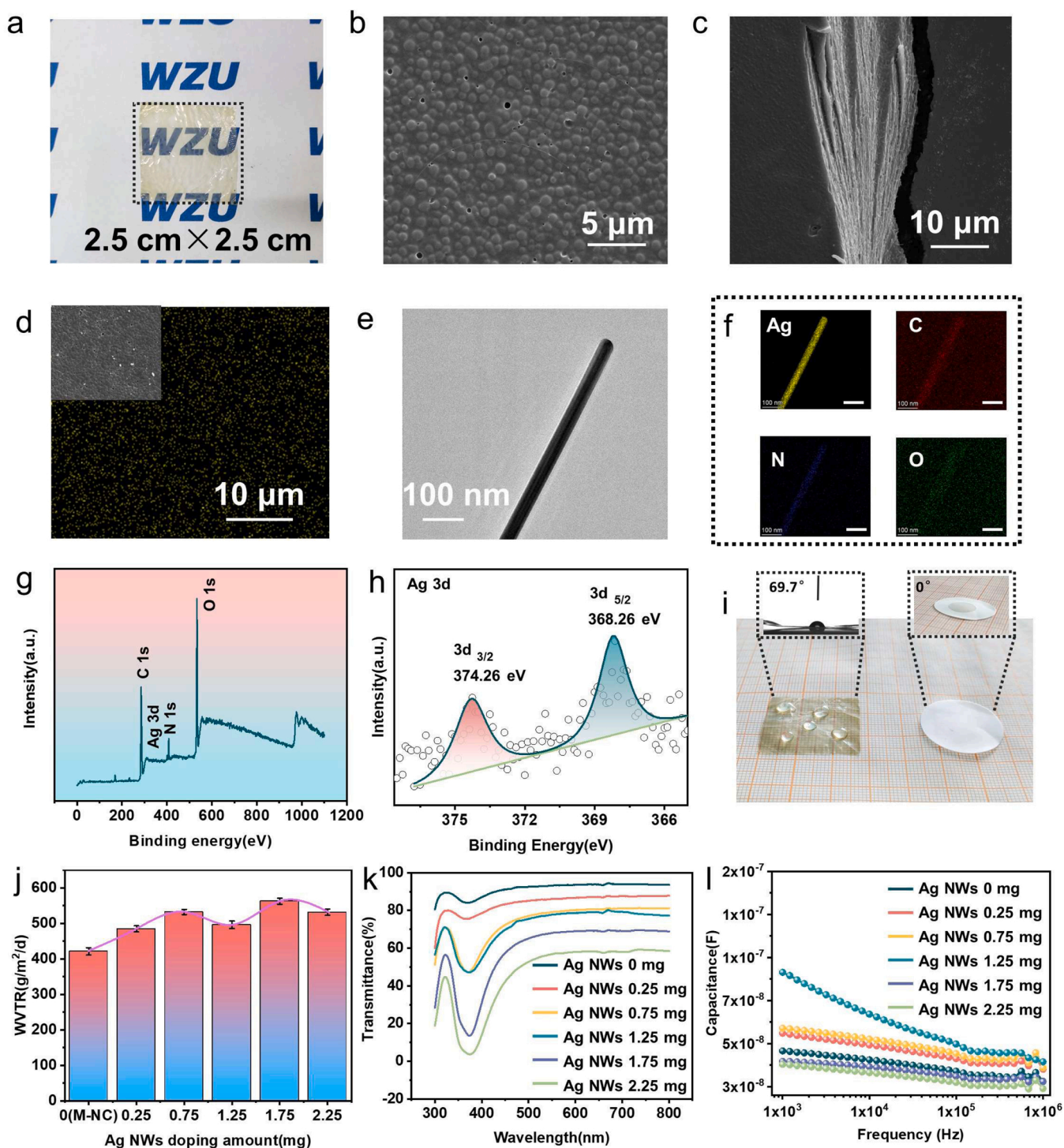


Fig. 2. Fabricated NC-Ag NWs, morphologies and other physical characteristics. (a) The prepared NC-Ag NWs. (b-c) The surface and section morphologies of NC-Ag NWs (10 μm). (d) The EDS results of Ag element and the corresponding surface morphology of NC-Ag NWs. (e) The TEM image of Ag NW distributed in NC-Ag NWs. (f) The EDS results of Ag NW in NC-Ag NWs, the scale is 100 nm. (g) The XPS full spectrum of NC-Ag NWs. (h) The Ag 3d XPS spectrum of NC-Ag NWs. (i) The waterproofness of NC-Ag NWs (water contact angle 69.7°) and pure NC. (j-l) The breathability, transmittance and capacitance of NC-Ag NWs.

Therefore, internal capacitances may generate between Ag NWs and NC. Two simple capacitance models are constructed to elucidate the mechanism better (Fig. S3). The capacitance of NC-Ag NWs can be enhanced due to the superposition of internal capacitance, while the capacitance of NC is a constant. In addition, the chemical composition of the NC-Ag NWs surface was investigated. The full XPS spectrum of NC-Ag NWs indicates the presence of the element C, O, N and Ag (Fig. 2g). The high-resolution spectrum of C 1s and N 1s is shown in Fig. S4. The

characteristic peaks of C 1s can be attributed to C-C/C-H (284.8 eV), C-O (286.4 eV), C-O-C (287.5 eV) and C=O (289.3 eV). The existence of -O-NO₂ (407.65 eV) in the N 1s [40,41]. The characteristic peaks of 368.26 eV and 374.26 eV indicate that a small part of Ag NWs is distributed on the surface of NC-Ag NWs (Fig. 2h) [42,43]. It should be noted that the spectrum of Ag 3d is small, which can attribute to the measured thin depth of XPS, and the surface of Ag NWs is covered by NC. Fig. S5 shows the XRD result of the NC-Ag NWs, the peak of NC in NC-Ag

NWs is about 20°, which is consistent with the previous study [44]. Furthermore, the XRD result of NC-Ag NWs turns out to be a cubic phase and shows main diffraction peaks at 38.2°, 44.4° and 64.6°, respectively, which is matched well with Ag (according to the ICDD PDF card 01-087-0718). The three diffraction peaks are ascribed to the (111), (200) and (220) of Ag [45]. In order to investigate the thermal stability of NC-Ag NWs, the thermogravimetric analysis was performed (Fig. S6). The temperature of the experiments was 40–600 °C. For the sample of NC-Ag NWs (0 mg Ag NWs), the weight is decreased slightly between 120 and 180 °C, which can ascribe to the denitration reaction of NC molecule. The weight is reduced dramatically when the temperature is about 180 °C corresponds to the autocatalytic reaction of NC driven by the escaping NO₂ gas [46]. The weight loss rate of the sample is 96.2% when the temperature is 400 °C and trend to be stable. The thermal decomposition process of NC-Ag NWs is similar to the film of no Ag NWs. But the denitration temperature of NC-Ag NWs is lower than NC-Ag NWs (0 mg Ag NWs) and the weight loss rates are declined with the increase of Ag NWs. The reason can ascribe to the samples doped Ag NWs possess high thermal absorption therefore the NC can be decomposed quickly.

The difference in waterproofness between pure NC and NC-Ag NWs was displayed in Fig. 2i and Video S1. The water drops were absorbed into the internal of NC membrane within seconds due to the diffusion effect, while the water drops on the NC-Ag NWs surface were suspended. The water contact angle of NC-Ag NWs doped Ag NWs of 1.25 mg is 69.7°. The water contact angle of NC-Ag NWs shows an upward trend with the increase of Ag NWs (Fig. S7). The excellent waterproofness of NC-Ag NWs indicates that the NC-Ag NWs can prevent water from surface infiltrates to electrode. Fig. S8 presents the breathability of the NC-Ag NWs, water vapor can pass the NC-Ag NWs and attach to the large beaker wall due to the nano/micro-pores of NC-Ag NWs. On the contrary, water vapor cannot pass through the plastic wrap. To quantitatively study the breathability of NC-Ag NWs, control experiments of water vapor transmission rate (WVTR) based on Fiskian diffusion (Note S1) were conducted at the same environment (Temperature: 293 K, relative humidity: 40%). As shown in Fig. 2j, the WVTR of NC-Ag NWs was improved slightly with the increase of the Ag NWs at the range of 0–2.25 mg.

Supplementary material related to this article can be found online at [doi:10.1016/j.nanoen.2023.108649](https://doi.org/10.1016/j.nanoen.2023.108649).

Apart from the good waterproofness and breathability, the transparency of NC-Ag NWs was also studied in this report. Typically, it is hardly transparent for a pure NC membrane (Shown in Fig. S9). The transmittance of modified NC (with 0 mg Ag NWs) can reach 92% (Fig. 2k). But the transmittance shows a downward tendency as the content of Ag NWs increased (Fig. 2k and Fig. S9).

For contact-separation TENG, the internal capacitance of friction layer plays a great part in output performance [47]. Fig. 2l shows the capacitance of NC-Ag NWs with different contents of Ag NWs at various frequencies, the details of the calculation can be found in Note S2 [48]. As the doped content of Ag NWs increases, the capacitance of NC-Ag NWs shows the same trend at the beginning. However, increase of Ag NWs steadily leads to a decrease of capacitance. For the sake of investigating the role of Ag NWs in improving the performance of TENG, calculation and simulation were conducted with COMSOL Multiphysics software 5.6.

The capacitance of TENG can be expressed as:

$$C = \frac{\epsilon_0 \epsilon_r S}{d} \quad (1)$$

Where ϵ_0 , ϵ_r is the vacuum dielectric constant and NC-Ag NWs dielectric constant, respectively, S represents the area of NC-Ag NWs (excluding the area of micro/nano-pores), d is the thickness of NC-Ag NWs. The capacitance of NC-Ag NWs is changed with the increase of Ag NWs. Ideally, Ag NWs are distributed homogeneously in NC. Due to the multi-layered structure and breathability of NC-Ag NWs, supposing the NC

that doped Ag NWs are embedded in n -layer NC-Ag NWs (Fig. 3a).

The capacitance of NC-Ag NWs can be expressed as:

$$C = \frac{\epsilon_0 \epsilon_r A}{d} + \frac{\epsilon_0 \epsilon_{r1} (S - A)}{d} + \frac{n \epsilon_0 S}{l - nd} \quad (2)$$

Where d is the length of every layer, ϵ_{r1} is the relative dielectric constant of Ag NWs. A represents the real surface area of NC, thus $S - A$ is the surface area of Ag NWs, which has a close relation with the number of Ag NWs. Supposing m is the number of Ag NWs of one layer, taking m as $S - A$ can simplify the calculation.

$$C = \frac{\epsilon_0 \epsilon_r A}{d} + \frac{\epsilon_0 \epsilon_{r1} m}{d} + \frac{n \epsilon_0 S}{l - nd} \quad (3)$$

The first term of Eq. (3), stands for the capacitance of pure NC-based TENG device, the second term is the enhanced capacitance by doping Ag NWs, and the third term represents the capacitance of interlayer air. The relationships between S , A , n , d , m and l and C can be illustrated clearly by Eq. (3), at ideal condition, supposing n , d , l and S are constant, C raises with the increase of m thus the output performance of TENG may show the same tendency. But increases the content of Ag NWs steadily, some Ag NWs are lapped with previous Ag NWs (Fig. S10). Supposing the amount of overlapped Ag NWs is a ($a < m$) in one layer, the capacitance of NC-Ag NWs can be defined as:

$$C = \frac{\epsilon_0 \epsilon_r A}{d} + \frac{\epsilon_0 \epsilon_{r1}}{d} (m - a) + \frac{n \epsilon_0 S}{l - nd} \quad (4)$$

Seen from Eq. (4), C is enhanced further when the content of Ag NWs is increased until the critical point. Normally, those Ag NWs have no structured distribution in NC-Ag NWs, on the contrary, those nanowires are distributed randomly. Supposing the inherent characteristics of Ag NWs and NC-Ag NWs are constant (A , n , l , d , S). With the increase of Ag NWs, m may decrease gradually due to the sharp increase of a , until $(m - a)$ is close to one, and the C of NC-Ag NWs is appeared the same tendency. It should be noted that the edge effect and charges leakage of NC-Ag NWs are not considered in the model. Based on the model of NC-Ag NWs, corresponding simulation was conducted and the external voltage of this capacitance model was set as 1.0V. The results are shown in Fig. 3b-g and Table S1, which indicates that the capacitance value shows an increased trend until the aggregation is happened in NC-Ag NWs.

Based on the discussion above, a TENG with vertical contact-separation mode was designed to further test the role of Ag NWs in improving the triboelectric performance of TENG, Fig. 3h illustrates the structure and operation mechanism of NC-TENG. The NC-Ag NWs membrane acted as the positive friction layer, while PDMS was selected as the negative friction layer due to its superior negative polarity and softness, also, Al is selected as a mental electrode of the negative friction layer while the conductive fabric was the electrode of the positive friction layer to endow the breathability of the device. At the beginning, there is no charges and potential difference between NC-Ag NWs and PDMS. When the NC-Ag NWs and PDMS are contacted under the action of external force, positive and negative charges are generated at the surface of contacted area due to the contact electrification effect. As the external force is released, the potential difference is increased gradually as the increase of separation distance. Correspondingly, the instantaneous current is generated at that moment of the two friction layers begin to separate. When the two materials are approaching under the effect of external force, charges are transferred with opposite direction, which leads to a contrary instantaneous current. Contact and separation cyclically can generate periodical triboelectric signal.

The NC-Ag NWs was cut as 3 cm × 3 cm to test the triboelectric output performance. The results of the finite element analysis of the TENG were shown in Fig. S11. The external force of friction layers was generated by a linear motor with a constant frequency of 1 Hz at the separation distance of 2 cm and the triboelectric signal was collected by an electrometer. In addition, some control experiments were conducted, when the content of added Ag NWs was tiny (0.25 mg), those Ag NWs

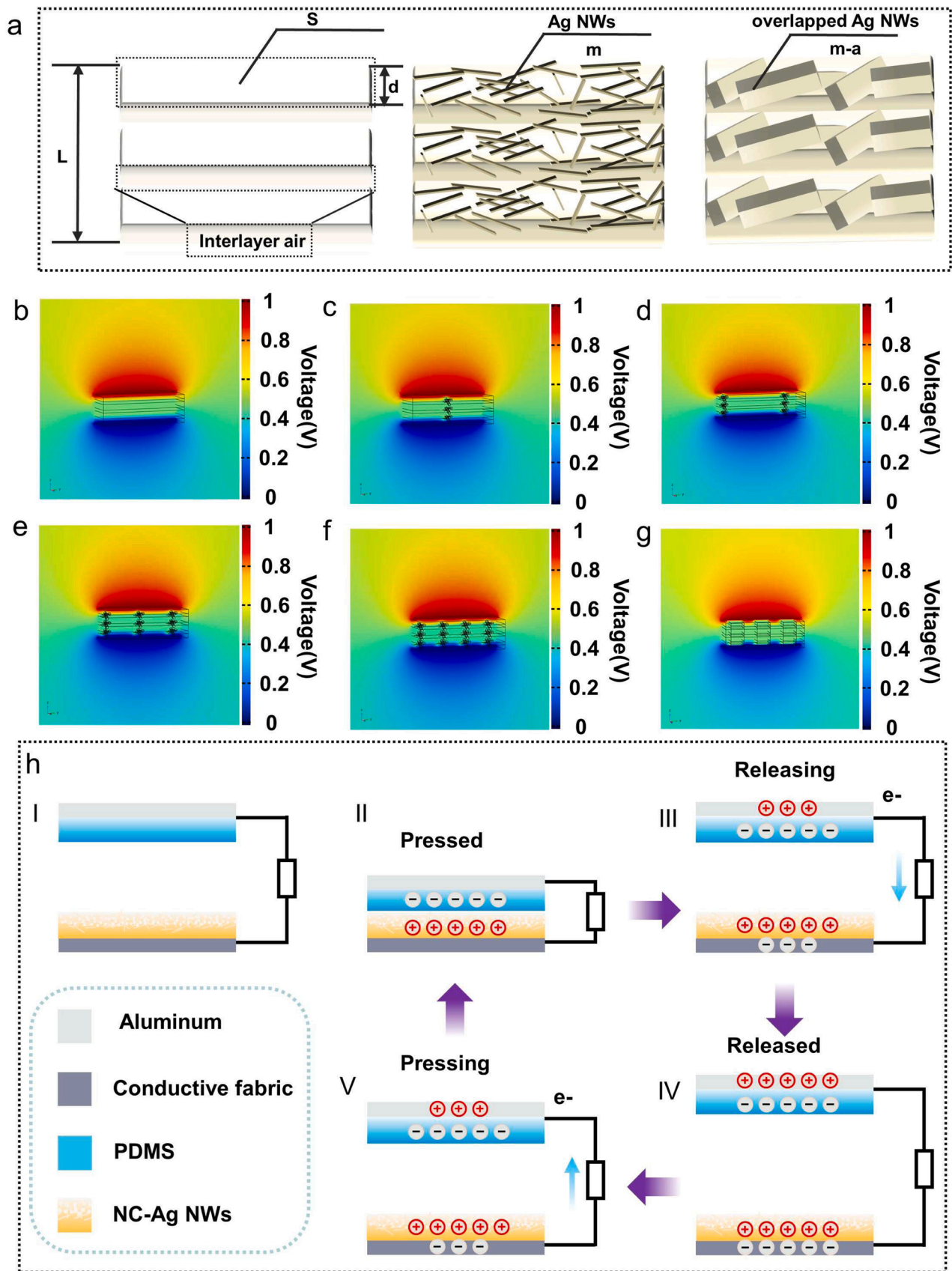


Fig. 3. Calculation model, charges transfer mechanism and simulation results of internal capacitance model of NC-TENG. (a) Calculation model of NC-Ag NWs. (b) Pure NC membrane. (c) A little Ag NWs filled in NC membrane. (d) A small of Ag NWs filled in NC membrane. (e) Some Ag NWs filled in NC membrane. (f) A lot of Ag NWs Filled in NC membrane. (g) Ag NWs agglomeration occurs in membrane. (h) Schematic of the working mechanism.

could distribute uniformly in NC-Ag NWs. Fig. 4a, b and c exhibit the open-circuit voltage, transferred charges and short-circuit current of NC-TENG with different contents of Ag NWs. As the increase of Ag NWs, the output performance of TENG shows a marked raise. However, the output performance displays a sharp decrease when the content of Ag NWs

increases steadily, which is ascribed to the overlapped three-dimensional structure and aggregation of Ag NWs in NC-Ag NWs. However, the aggregated of Ag NWs in NC-Ag NWs leads to the reduction of dielectric characteristic [49]. As a proof of concept, the SEM photographs of NC-Ag NWs with different Ag NWs, from 0.25 mg to

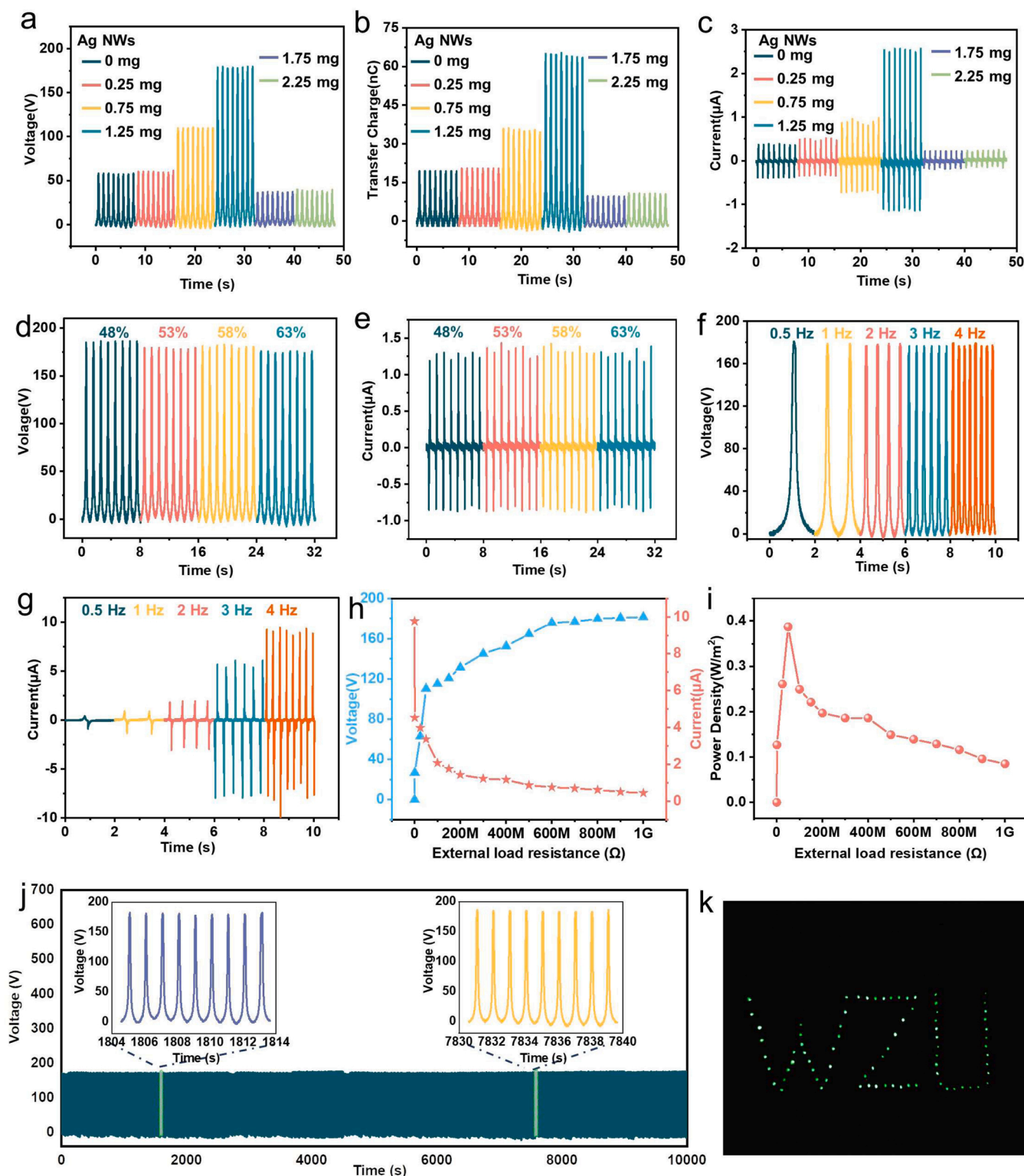


Fig. 4. The electrical output performance of NC-TENG, stability. (a–c) Open-circuit voltages, transfer charge quantities and short-circuit current, respectively. (d) Open-circuit voltages at RH 48%–63%. (e) short-circuit current at RH 48%–63%. (f) Open-circuit voltages at exerted frequency 0.5–4 Hz. (g) short-circuit current at exerted frequency 0.5–4 Hz. (h) The output voltage and current under varied external load resistance. (i) Power densities at the varied external load resistance. (j) The open-circuit voltages at 10000 times circles at 1 Hz frequency. (k) Green LEDs lighted by NC-TENG.

2.25 mg were shown in Fig. S12. When the content of Ag NWs is increased steadily, the three-dimensional structure of Ag NWs also shown an increase tendency. However, while the doped content of Ag NWs is over 1.25 mg, the overlapping three-dimensional structure and aggregation are generated in NC-Ag NWs (Fig. S13), which contributes to the Ag NWs no longer distribution homogeneously thus leading to the decrease of output performance of NC-TENG. The experimental results show the same trend with the simulation results.

NC-Ag NWs doped 1.25 mg of Ag NWs have the best output performance, which was chosen as the optimal sample for further study. The humidity of the environment is a significant factor for TENG performance [50], high humidity causes a decrease in output performance as usual. The output performance of NC-TENG at different relative humidity (RH) is discussed and the results are shown in Fig. 4d and Fig. 4e. The output voltage is decreased slightly with the increase of humidity from 48% to 63%. The stable output performance of NC-TENG in a humidity environment is attributed to the outstanding waterproofness, which indicates the NC-TENG can operate in changeable RH. Besides, the output performance of NC-TENG at different frequencies (0.5–4 Hz) was studied (Fig. 4f–g). The open-circuit voltage is almost stable, while the short-circuit current presents a growth tendency. The relation between loading frequency and output performance is demonstrated in Fig. S14 and Note S3 [51].

The open-circuit voltage and short-circuit current of NC-TENG are measured with the external load resistance changes from 10 MΩ to 1 GΩ. As the external load resistance increase, the open-circuit voltage displays an upward tendency, while the short-circuit current shows an opposite trend, which results indicate that the triboelectric output of NC-TENG also obeys Ohm's law (Fig. 4 h). The output power is calculated by the following equation:

$$P = UI \quad (5)$$

Where U is the output voltage and I is the instantaneous current, respectively. The maximum output power density of NC-TENG can reach 0.38 W/m^2 when the external load resistance is 50 MΩ (Fig. 4i).

Furthermore, the output voltage still keeps stable after placing the NC-TENG in air (relative humidity is 63%) for 30 days, which shows the outstanding durability of NC-TENG (Fig. S15). Besides, the stability of NC-TENG is estimated by contact and separation of 10000 times at 1 Hz frequency, the output voltage has no obvious change with the increase of operation times (Fig. 4j). Table S2 exhibits the comparison between this work and the other breathable and waterproof reports, indicating the output performance of NC-TENG is adequate to prepare self-powered sensing device with high-performance.

To investigate the practical application of NC-TENG, some light-emitting diodes (LEDs) were connected (Fig. 4k). The NC-TENG was able to light 206 LEDs with periodic contact and separation of the two triboelectric layers (Fig. S16 and Video S2). To further study the sensing mechanism and broaden the application of NC-TENG, a SNC-TENG was designed to realize human-machine interaction. The structure and functional schematic are shown in Fig. 5a. The SNC-TENG was constituted of NC-Ag NWs and conductive fabric, a piece of PDMS as negative triboelectric layer. The working mechanism of SNC-TENG is shown in Fig. S17 and Note S4. According to the mechanism of SNC-TENG discussed above, analog signal can be generated when finger contacts with SNC-TENG (Fig. 5b). Fig. 5c provides the diagram of the whole human-machine interaction's process. Firstly, the analog signal is generated by SNC-TENG and is transmitted to a self-designed signal acquisition circuit for data pre-processing. Secondly, the pre-processing signal is transmitted to analog-to-digital converter (ADC) unit of microprocessor (MCU), where the signal is obtained and processed further by the MCU. Thirdly, features of the signal are extracted by a functional algorithm, the processed signal can be transmitted to the computer or other electric devices by serial communication in real-time for HMI.

Supplementary material related to this article can be found online at

[doi:10.1016/j.nanoen.2023.108649](https://doi.org/10.1016/j.nanoen.2023.108649).

Based on the above work, as a verification of the SNC-TENG for human-machine interaction, a TENG media interface was designed. As shown in Video S3 and Fig. S18, the media player of a computer could be controlled by SNC-TENG. Furthermore, LEDs lights were controlled by using those features that generated by a finger touched with SNC-TENG, such as contact time and pressure. And those feature data of SNC-TENG pressured by finger were exhibited in Fig. 5d–i. The circuit of the LEDs lights was depicted in Fig. S19, and the SNC-TENG was connected to the signal acquisition circuit and served as an input port. Seen from Fig. 5d and Fig. 5e, in which signals with different pressure or frequency can be distinguished clearly. In addition, the response time of SNC-TENG at 1 Hz frequency was investigated. The response time is 130 ms and recovery time is 100 ms (Fig. S20), which indicates the SNC-TENG can response external force timely. Also, as shown in Fig. 5f–g and Video S4–5, features of triboelectric signals can be extracted by MCU to control the brightness and twinkle frequency of LEDs lights, respectively. The LEDs lights were lightened or darkened gradually due to the contact between finger and SNC-TENG with different pressures (Fig. 5f and Fig. 5g). In addition, due to the electrons are still kept on the surface of the friction layer when two friction layers are contacted, thus the voltage is not changed immediately until two friction layers begin to separate. By extracting the retention time of voltage, the twinkle frequency of LEDs lights can be controlled by a finger. Also, immersive experience of human-machine interaction can be realized by combining the pressure and retention time of finger touch at the same time. The brightness and twinkle frequency of LEDs lights can be controlled at the same time by SNC-TENG (Fig. 5h–i).

Supplementary material related to this article can be found online at [doi:10.1016/j.nanoen.2023.108649](https://doi.org/10.1016/j.nanoen.2023.108649).

Compared with single sensing unit, the matrix keyboard consisted of multiple sensing units shows more advantages in HMI [52–55]. In addition, the matrix keyboard based on the principle of double electrode can improve the sensing performance and release hardware resource. To reduce the redundancy of hardware design and broaden the interaction mode of NC-TENG in wearable devices, a 3×3 matrix keyboard is fabricated (Fig. 6a–c). The structure and size of the matrix keyboard is shown in Fig. 6b. The matrix keyboard consisted of two layers, including a bottom and a top layer, each layer contained three channels for data acquisition (Fig. 6c). The matrix keyboard can record two types of features at the same time, such as touch pressure and touch time of the finger, which can be used to achieve multiple HMI. Furthermore, for the sake of recording the triboelectric signals of six channels concurrently, a six channels triboelectric signal acquisition circuit was designed with the help of printed circuit board (PCB) technology (Fig. S21). The diagram of data acquisition from the TENG matrix keyboard was illustrated in Fig. S22. The data acquisition circuit was mainly consisted of two parts, including an operational amplifier for acquiring data and a second order low pass filter for filtering slight vibration. When a finger touched to one of the keyboard units of TENG, two triboelectric signals with opposite potential were generated (Fig. S23). It is worth noting that triboelectric signals were not totally inverse, which may ascribe to the triboelectric performance between positive and negative triboelectric is differentiated.

From the system level, the triboelectric signals of matrix keyboard were collected in real-time by an acquisition circuit and transmitted to MCU. To broaden the application of human-machine interaction, a Thin Film Transistor (TFT) screen was used to visualize the touch result. Fig. 6d–g illustrates the triboelectric signals and the corresponding display results. From Fig. 6d and Video S6, opposite triboelectric signals were generated by the finger touch, those features, such as press time and pressure can be recorded. When finger pressed a “T” on the matrix keyboard, the corresponding letters can be displayed on the TFT screen simultaneously. By the same measure, many letters or numbers can be displayed by this device.

Supplementary material related to this article can be found online at

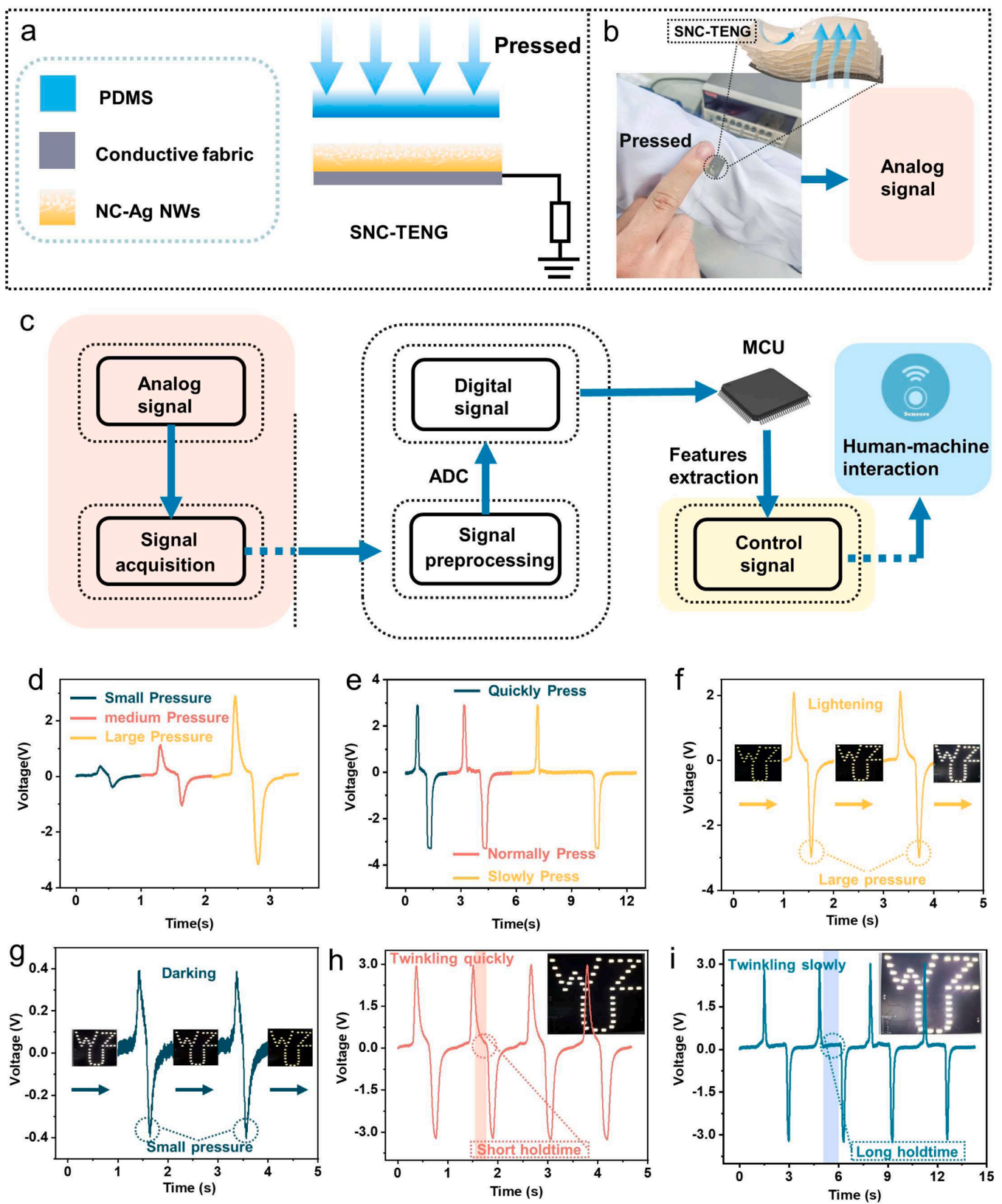


Fig. 5. Structure, signal processing, and sensing performance of SNC-TENG. (a) Schematic diagram of SNC-TENG. (b) Process of signal acquisition. (c) signal processing of SNC-TENG. (d-e) Different pressure and press times of humans touched with SNC-TENG. (f) The LEDs light lightened by SNC-TENG gradually. (g) The LEDs light darkens by SNC-TENG gradually. (h-i) The LEDs light twinkles quickly and slowly due to the different touch times.

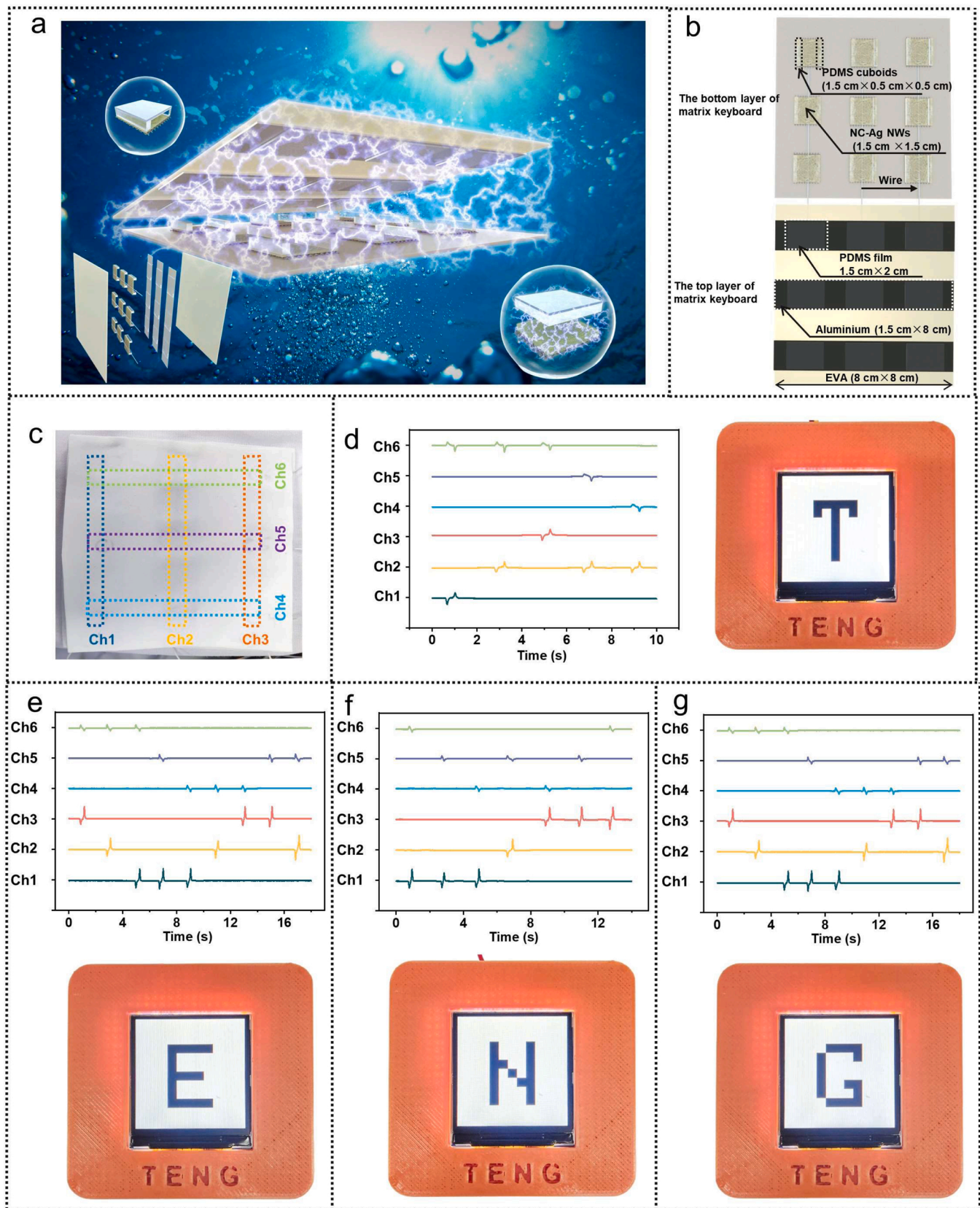


Fig. 6. The diagram of double electrode 3 × 3 matrix keyboard, sensing signal at a real-time and display results. (a) The whole structure diagram of the 3 × 3 matrix keyboard. (b) Top layer and bottom layer of fabricated double electrode matrix keyboard. (c) Working diagram of double electrode matrix keyboard. (d) Signal features of “T” and the display result correspondingly. (e) Signal features of “E” and the display result correspondingly. (f) Signal features of “N” and the display result correspondingly. (g) Signal features of “G” and the display result correspondingly.

doi:10.1016/j.nanoen.2023.108649.

4. Conclusion

In summary, a waterproof and breathable TENG was demonstrated in this paper using a cost-effective and viable method. And NC-Ag NWs was fabricated for the tribo-positive layer, which exhibited favorable waterproofness (WCA: 86.9°), breathability (WVTR: 562.62 g/m²/d) and transparency (92%). In addition, the triboelectric performance of pure NC can be enhanced by doping a certain content of Ag NWs, and the enhanced mechanism was validated by the internal capacitance modeling of NC-Ag NWs and experimental results. The output voltage increased from 50 V to 180 V, and the transferred charges were increased from 18 nC to 68 nC. The maximum instantaneous power density was 0.38 W/m² at the separation distance was 2 cm. Furthermore, a self-powered sensing device based on SNC-TENG was fabricated for HMI, features of touch pressure and touch time could be extracted at the same time, which enabled the diverse interactive with electric devices. We also designed a matrix keyboard based on the double electrode TENG, which could record touch process and visualize touch result. This work offers promising prospects for both wearing comfort and high-performance of TENG sensing devices. The fabricated TENGs have significant potential as human-machine interfaces, wearable devices, and electronic skins (e-skins).

CRediT authorship contribution statement

Tong Zheng and Guizhong Li: Conceptualization, Writing – original draft preparation, Methodology, Investigation. **Linnan Zhang:** Construction of test platform. **Weifang Sun, Xiaoming Pan, Taihong Chen, Yuanhao Wang, Yuqing Zhou, Jili Tian and Ya Yang:** Supervision, Validation, Writing-Reviewing, Revising and Editing. All authors contributed to data analysis and commented on the manuscript.

Declaration of Competing Interest

The authors declare that they have no known competing financial interests or personal relationships that could have appeared to influence the work reported in this paper.

Data availability

Data will be made available on request.

Acknowledgment

This work was supported by Wenzhou Association for Science and Technology (grant No. jczc156); The Graduate Scientific Research Foundation of Wenzhou University (Grant No. XK230429); Wenzhou science and Technology Bureau of China (Wenzhou major scientific and technological innovation project under Grant No. ZG2020029); National Natural Science Foundation of China (Grant No. 52202213); Natural Science Foundation of Shandong Province (Grant No. ZR2021QE210), and Zhejiang Province “Leading Wild Goose” Research and Development Plan Project (Grant No. 2022C01SA371652).

Appendix A. Supporting information

Supplementary data associated with this article can be found in the online version at doi:10.1016/j.nanoen.2023.108649.

References

- [1] Y.R. Yang, W. Gao, Wearable and flexible electronics for continuous molecular monitoring, *Chem. Soc. Rev.* 48 (2019) 1465–1491.

- [2] G. Yao, L. Xu, X.W. Cheng, Y.Y. Li, X. Huang, W. Guo, S.Y. Liu, Z.L. Wang, H. Wu, Bioinspired triboelectric nanogenerators as self-powered electronic skin for robotic tactile sensing, *Adv. Funct. Mater.* 30 (2020), 1907312.
- [3] X. Peng, K. Dong, C.Y. Ye, Y. Jiang, S.Y. Zhai, R.W. Cheng, D. Liu, X.P. Gao, J. Wang, Z.L. Wang, A breathable, biodegradable, antibacterial, and self-powered electronic skin based on all-nanofiber triboelectric nanogenerators, *Sci. Adv.* 6 (2020) 9624.
- [4] M. Pan, C.G. Yuan, X.R. Liang, J. Zou, Y. Zhang, C. Bowen, Triboelectric and piezoelectric nanogenerators for future soft robots and machines, *iScience* 23 (2020), 101682.
- [5] Y.H. Zhou, X. Xiao, G.R. Chen, X. Zhao, J. Chen, Self-powered sensing technologies for human Metaverse interfacing, *Joule* 6 (2022) 1381–1389.
- [6] X. Peng, K. Dong, Y.F. Zhang, L.L. Wang, C.H. Wei, T.M. Lv, Z.L. Wang, Z.Y. Wu, Sweat-permeable biodegradable transparent and self-powered chitosan-based electronic skin with ultrathin elastic gold nanofibers, *Adv. Funct. Mater.* 32 (2022), 2112241.
- [7] H.S. Niu, H. Li, S. Gao, Y. Li, X. Wei, Y.K. Chen, W.J. Yue, W.J. Zhou, G.Z. Shen, Perception-to-cognition tactile sensing based on artificial-intelligence-motivated human full-skin bionic electronic skin, *Adv. Mater.* 34 (2022), 2202622.
- [8] Y. Luo, Z.H. Wang, J.Y. Wang, X. Xiao, Q. Li, W.B. Ding, H.Y. Fu, Triboelectric bending sensor based smart glove towards intuitive multi-dimensional human-machine interfaces, *Nano Energy* 89 (2021), 106330.
- [9] C.Y. Li, D. Liu, C.Q. Xu, Z.M. Wang, S. Shu, Z.R. Sun, W. Tang, Z.L. Wang, Sensing of joint and spinal bending or stretching via a retractable and wearable badge reel, *Nat. Commun.* 12 (2021) 2950.
- [10] F.L. He, X.Y. You, H. Gong, Y. Yang, T. Bai, W.G. Wang, W.X. Guo, X.Y. Liu, M. D. Ye, Stretchable, biocompatible, and multifunctional silk fibroin-based hydrogels toward wearable strain/pressure sensors and triboelectric nanogenerators, *ACS Appl. Mater. Interfaces* 12 (2020) 6442–6450.
- [11] H. Lei, H.F. Ji, X.H. Liu, B.H. Lu, L.J. Xie, E.G. Lim, X. Tu, Y. Liu, P.X. Zhang, C. Zhao, X. Sun, Z. Wen, Self-assembled porous-reinforcement microstructure-based flexible triboelectric patch for remote healthcare, *Nano-Micro Lett.* 15 (2023) 109.
- [12] R.Y. Zhang, C. Dahlstrom, H.Y. Zou, J. Jonzon, M. Hummelgard, J. Ortegren, N. Blomquist, Y. Yang, H. Andersson, M. Olsen, M. Norgren, H. Olin, Z.L. Wang, Cellulose-based fully green triboelectric nanogenerators with output power density of 300 W/m², *Adv. Mater.* 32 (2020), 2002824.
- [13] B.D. Chen, Z.L. Wang, Toward a new era of sustainable energy: advanced triboelectric nanogenerator for harvesting high entropy energy, *Small* 18 (2022), 2107034.
- [14] Z.L. Wang, On Maxwell's displacement current for energy and sensors: the origin of nanogenerators, *Mater. Today* 20 (2017) 74–82.
- [15] J.J. Luo, W.C. Gao, Z.L. Wang, The triboelectric nanogenerator as an innovative technology toward intelligent sports, *Adv. Mater.* 33 (2021), 2004178.
- [16] J.P. Wu, Y. Zheng, X.Y. Li, Recent progress in self-powered sensors based on triboelectric nanogenerators, *Sensors* 21 (2021) 7129.
- [17] F.R. Fan, Z.Q. Tian, Z.L. Wang, Flexible triboelectric generator, *Nano Energy* 1 (2012) 328–334.
- [18] S.W. Chen, S.M. Huang, H.S. Wu, W.P. Pan, S.M. Wei, C.W. Peng, I.C. Ni, B. T. Murti, M.L. Tsai, C.I. Wu, P.K. Yang, Fabric Compatible, and flexible borophene nanocomposites for self-powered smart assistive and wound healing applications, *Adv. Sci.* 9 (2022), 2201507.
- [19] M.A.F. Angeles, M. Lopez-Lopez, M. Torre, C. Garcia-Ruiz, Analytical techniques in the study of highly-nitrated nitrocellulose, *Trac-Trends Anal. Chem.* 30 (2012) 1740–1755.
- [20] W.Y. Wei, Y.P.Q. Yi, J. Song, X.G. Chen, J.H. Li, J.S. Li, Tunable graphene/nitrocellulose temperature alarm sensors, *ACS Appl. Mater. Interfaces* 14 (2022) 13790–13800.
- [21] L.R. Tang, W.X. Chen, B. Chen, R.X. Lv, X.Y. Zheng, C. Rong, B.L. Lu, B. Huang, Sensitive and renewable quartz crystal microbalance humidity sensor based on nitrocellulose nanocrystals, *Sens. Actuators B-Chem.* 327 (2020), 128944.
- [22] R.H. Tang, M.Y. Xie, M. Li, L. Cao, S.S. Feng, Z.D. Li, F. Xu, Nitrocellulose membrane for paper-based biosensor, *Appl. Mater. Today* 26 (2022), 101305.
- [23] Y. Jie, H.R. Zhu, X. Cao, Y. Zhang, N. Wang, L.Q. Zhang, Z.L. Wang, One-piece triboelectric nanosensor for self-triggered alarm system and latent fingerprint detection, *ACS Nano* 10 (2016) 10366–10372.
- [24] S. Chen, J.X. Jiang, F. Xu, S.Q. Gong, Crepe cellulose paper and nitrocellulose membrane-based triboelectric nanogenerators for energy harvesting and self-powered human-machine interaction, *Nano Energy* 61 (2019) 69–77.
- [25] Y.P. Shi, X.L. Wei, K.M. Wang, D.D. He, Z.H. Yuan, J.H. Xu, Z.Y. Wu, Z.L. Wang, Integrated all-fiber electronic skin toward self-powered sensing sports systems, *ACS Appl. Mater. Inter.* 13 (2021) 50329–50337.
- [26] I. Kim, H. Jeon, D. Kim, J. You, D. Kim, All-in-one cellulose based triboelectric nanogenerator for electronic paper using simple filtration process, *Nano Energy* 53 (2018) 975–981.
- [27] X. Peng, K. Dong, Y.F. Zhang, L.L. Wang, C.H. Wei, T.M. Lv, Z.L. Wang, Z.Y. Wu, Sweat-permeable, biodegradable, transparent and self-powered chitosan-based electronic skin with ultrathin elastic gold nanofibers, *Adv. Funct. Mater.* 32 (2022), 2112241.
- [28] D.J. Lu, T. Liu, X.J. Meng, B. Luo, J.X. Yuan, Y.H. Liu, S. Zhang, C.C. Cai, C. Gao, J. L. Wang, S.F. Wang, S.X. Nie, Wearable triboelectric visual sensors for tactile perception, *Adv. Mater.* 35 (2023), 2209117.
- [29] G.L. Du, J.L. Wang, Y.H. Liu, J.X. Yuan, T. Liu, C.C. Cai, B. Luo, S.Q. Zhu, Z.T. Wei, S.F. Wang, S.X. Nie, Fabrication of advanced cellulosic triboelectric materials via dielectric modulation, *Adv. Sci.* 10 (2023), 2206243.

- [30] J.Y. Huang, Y. Hao, M. Zhao, W. Li, F.L. Huang, Q.F. Wei, All-fiber-structured triboelectric nanogenerator via one-pot electrospinning for self-powered wearable sensors, *ACS Appl. Mater. Interfaces* 13 (2021) 21774–24784.
- [31] H.Y. Xu, J. Tao, Y. Liu, Y.P. Mo, R.R. Bao, C.F. Pan, Fully fibrous large-area tailorable triboelectric nanogenerator based on solution blow spinning technology for energy harvesting and self-powered sensing, *Small* 18 (2022), 2202477.
- [32] Y. Li, S. Xiao, X.X. Zhang, P. Jia, S.S. Tian, C. Pan, F.P. Zeng, D.C. Chen, Y.Y. Chen, J. Tang, J.Q. Xiong, Silk inspired in-situ interlocked superelastic microfibers for permeable stretchable triboelectric nanogenerator, *Nano Energy* 98 (2022), 107347.
- [33] L.Y. Lan, J.Q. Xiong, D.C. Gao, Y. Li, J. Chen, J. Lv, J.F. Ping, Y.B. Ying, P.S. Lee, Breathable nanogenerators for an on-plant self-powered sustainable agriculture system, *ACS Nano* 15 (2021) 5307–5315.
- [34] H.L. Wang, Z.H. Guo, X. Pu, Z.L. Wang, Ultralight iontronic triboelectric mechanoreceptor with high specific outputs for epidermal electronics, *Nano-Micro Lett.* 14 (2022) 86.
- [35] C.Y. Ye, D. Liu, X. Peng, Y. Jiang, R.W. Cheng, C. Ning, F.F. Sheng, Y.H. Zhang, K. Dong, Z.L. Wang, A hydrophobic self-repairing power textile for effective water droplet energy harvesting, *ACS Nano* 15 (2021) 18172–18181.
- [36] S.N. Cui, L.L. Zhou, D. Liu, S.X. Li, L. Liu, S.Y. Chen, Z.H. Zhao, W. Yuan, Z. L. Wang, J. Wang, Improving performance of triboelectric nanogenerators by dielectric enhancement effect, *Matter* 5 (2022) 180–193.
- [37] H.Y. Wu, W.C. He, C.C. Shan, Z. Wang, S.K. Fu, Q. Tang, H.Y. Guo, Y. Du, W.L. Liu, C.G. Hu, Achieving remarkable charge density via self-polarization of polar high-k material in a charge-excitation triboelectric nanogenerator, *Adv. Mater.* 34 (2022), 2109918.
- [38] K.M. Shi, H.Y. Zou, B. Sun, P.K. Jiang, J.L. He, X.Y. Huang, Dielectric modulated cellulose paper/PDMS-based triboelectric nanogenerators for wireless transmission and electropolymerization applications, *Adv. Funct. Mater.* 30 (2020), 1904536.
- [39] J. Chen, H.Y. Guo, X.M. He, G.L. Liu, Y. Xi, H.F. Shi, C.G. Hu, Enhancing performance of triboelectric nanogenerator by filling high dielectric nanoparticles into sponge PDMS film, *ACS Appl. Mater. Interfaces* 8 (2016) 736–744.
- [40] Y. Luo, T.Y. Li, H.Z. Zhang, W. Liu, X.B. Zhang, J.W. Yan, H.M. Zhang, X.F. Li, Endogenous symbiotic Li3N/cellulose skin to extend the cycle life of lithium anode, *Angew. Chem. Int. Ed.* 60 (2021) 11718–11724.
- [41] K.G.U.R. Kumarasinghe, W.C.H. Silva, M.D.A. Fernando, L. Palliyaguru, P. S. Jayawardena, M. Shimomura, S.S.N. Fernando, T.D.C.P. Gunasekara, P. M. Jayaweera, One-pot reducing agent-free synthesis of silver nanoparticles/nitrocellulose composite surface coating with antimicrobial and antibiofilm activities, 2021, *Biomed. Res. Int.* (2021), 6666642.
- [42] X. Liu, Z.Q. Liu, J.L. Lu, X.L. Wu, B. Xu, W. Chu, Electrodeposition preparation of Ag nanoparticles loaded TiO2 nanotube arrays with enhanced photocatalytic performance, *Appl. Surf. Sci.* 288 (2014) 513–517.
- [43] L.T. Soo, K.S. Loh, A.B. Mohamad, W.R.W. Daud, W.Y. Wong, Synthesis of silver/nitrogen-doped reduced graphene oxide through a one-step thermal solid-state reaction for oxygen reduction in an alkaline medium, *J. Power Sources* 324 (2016) 412–420.
- [44] S. Chelouche, D. Trache, A.F. Tarchoun, K. Khimeche, A. Mezroua, Compatibility of nitrocellulose with aniline-based compounds and their eutectic mixtures, *J. Therm. Anal. Calorim.* 141 (2020) 941–955.
- [45] N. Li, G.W. Huang, X.J. Shen, H.M. Xiao, S.Y. Fu, Controllable fabrication and magnetic-field assisted alignment of Fe3O4-coated Ag nanowires via a facile coprecipitation method, *J. Mater. Chem. C* 1 (2013) 4879–4884.
- [46] X.J. Meng, Z.G. Xiao, Preparation and sensitivity property of nitrocellulose/silica composite with silica gel as coating layer, *Propellants Explos. Pyrotech.* 43 (2018) 999–1005.
- [47] Z.P. Zheng, Y.P. Guo, Dielectric modulated glass fiber fabric-based single electrode triboelectric nanogenerator for efficient biomechanical energy harvesting, *Adv. Funct. Mater.* 31 (2021), 2102431.
- [48] P.S.P.L. Taberna, P. Simon, J.F. Fauvarque, Electrochemical characteristics and impedance spectroscopy studies of carbon-carbon supercapacitors, *J. Electrochem. Soc.* 150 (2003) 292–300.
- [49] G.Z. Li, Y.W. Cai, G.G. Wang, N. Sun, F. Li, H.L. Zhou, X.N. Zhang, H.X. Zhao, Y. H. Wang, J.C. Han, Y. Yang, Performance enhancement of transparent and flexible triboelectric nanogenerator based on one-dimensionally hybridized copper/polydimethylsiloxane film, *Nano Energy* 99 (2022), 107423.
- [50] F. Jiang, X.R. Zhou, J. Lv, J. Chen, J.T. Chen, H. Kongcharoen, Y.H. Zhang, P. S. Lee, Stretchable, breathable, and stable lead-free perovskite/polymer nanofiber composite for hybrid triboelectric and piezoelectric energy harvesting, *Adv. Mater.* 34 (2022), 200042.
- [51] S.M. Niu, S.H. Wang, L. Lin, Y. Liu, Y.S. Zhou, Y.F. Hu, Z.L. Wang, Theoretical study of contact-mode triboelectric nanogenerators as an effective power source, *Energy Environ. Sci.* 6 (2013) 3576–3583.
- [52] Y.C. Lai, H.M. Wu, H.C. Lin, C.L. Chang, H.H. Chou, Y.C. Hsiao, Y.C. Wu, Entirely, intrinsically, and autonomously self-healable, highly transparent, and superstretchable triboelectric nanogenerator for personal power sources and self-powered electronic skins, *Adv. Funct. Mater.* 29 (2019), 1904626.
- [53] J.Y. Liu, Z. Wen, H. Lei, Z.Q. Gao, X.H. Sun, A liquid–solid interface-based triboelectric tactile sensor with ultrahigh sensitivity of 21.48 kPa–1, *Nano-Micro Lett.* 14 (2022) 88.
- [54] S.C. Zhang, Y. Xiao, H.M. Chen, Y.L. Zhang, H.Y. Liu, C.M. Qu, H.X. Shao, Y. Xu, Flexible triboelectric tactile sensor based on a robust MXene/leather film for human-machine interaction, *ACS Appl. Mater. Interfaces* 15 (2023) 13802–13812.
- [55] S. Shen, J. Yi, Z.D. Sun, Z.H. Guo, T.Y.Y. He, L.M. Li, J.J. Fu, C.K. Lee, Z.L. Wang, Human machine interface with wearable electronics using biodegradable

triboelectric films for calligraphy practice and correction, *Nano-Micro Lett.* 14 (2022) 255.



Tong Zheng is currently a Master student under supervision of Dr. Gui-Zhong Li at WenZhou University, China. His current research mainly focuses on the design and fabrication high-performance triboelectric devices for energy harvesting and self-powered sensing.



Dr. Guizhong Li received his Ph.D. in Materials Science and Engineering from Harbin Institute of Technology, China. He is currently a lecturer at WenZhou University, China. His research centers on the energy-harvesting devices based on flexible and transparent triboelectric nanogenerators.



Linnan Zhang is currently a Master student in WenZhou University of Mechanical and electric engineering, China. His research interests mainly focus on innovation and the design of hybrid triboelectric nanogenerator.



Dr. Weifang Sun received his Ph.D in aeronautics and astronautics engineering from Xiamen University, China. He is currently a lecture at WenZhou University, China. His research focuses on machine vision and manufacturing system inspection technology.



Xiaoming Pan is currently a Senior Experimentalist at WenZhou University, China. His research mainly focuses on detection technology and automation devices.



Associate Prof. Taihong Chen received his Ph.D. in mechanical and electric engineering from Chonnam National University, Korea. He is currently an associate professor at Wenzhou University, China. His research interests cover mechanical energy collection, mechanical structure design and control.



Associate Prof. Jili Tian received his PhD degree (2018) in materials science from Harbin Institute of Technology, Shenzhen. During 2018–2020, he has been a post-doctoral fellow at Xi'an Jiaotong University. Now he is an associate professor in college of energy and mechanical engineering, Dezhou University, China. His current research interests cover on the synthesis of nanomaterials and their applications in energy storage.



Prof. Yuanhao Wang received his Ph.D. in construction and environment engineering from Hong Kong Polytechnic University, China. He is currently a researcher at the Chinese Academy of Sciences and executive dean of Shenzhen Hoffman Advanced Materials Research Institute, China. His research interests cover environmental materials and engineering, nanomaterial for green buildings, solar energy materials, solar cells, lithium battery materials and devices.



Prof. Ya Yang received his Ph.D. in Materials Science and Engineering from University of Science and Technology Beijing, China. He is currently a professor at Beijing Institute of Nanoenergy and Nanosystems, Chinese Academy of Sciences, China. He has developed various new hybridized and multi-effects coupled nanogenerators, opening up new principles of the device design and coupled effects, and the new approaches of improving output performances of energy-related devices. His main research interests focus on the field of hybridized and coupled nanogenerators for energy conversion, self-powered sensing, and some new physical effects. Details can be found at: <http://www.researcherid.com/rid/A-7219-2016>.



Associate Prof. Yuqing Zhou received his Ph.D. in mechanical and electric engineering from Zhejiang University of Technology, China. He is currently an associate professor at Wenzhou University, China. His research focuses on status monitoring, fault diagnosis and machine learning.